Astronomy & Astrophysics

L<small>ETTER TO THE</small> E<small>DITOR</small>

Detection of buckminsterfullerene emission in the diffuse interstellar medium

O. Berné[1,2], N. L. J. Cox[1,2], G. Mulas[3], and C. Joblin[1,2]

[1] Université de Toulouse, UPS-OMP, IRAP, 31028 Toulouse, France
   e-mail: olivier.berne@gmail.com
[2] CNRS, IRAP, 9 Av. colonel Roche, BP 44346, 31028 Toulouse Cedex 4, France
[3] Istituto Nazionale di Astrofisica, Osservatorio Astronomico di Cagliari, strada 54, localit Poggio dei Pini, 09012 Capoterra (CA), Italy

ABSTRACT

Emission of fullerenes in their infrared vibrational bands has been detected in space near hot stars. The proposed attribution of the diffuse interstellar bands at 9577 and 9632 Å to electronic transitions of the buckminsterfullerene cation (i.e. C_{60}^+) was recently supported by new laboratory data, confirming the presence of this species in the diffuse interstellar medium (ISM). In this Letter, we present the detection, also in the diffuse ISM, of the 17.4 and 18.9 μm emission bands commonly attributed to vibrational bands of neutral C_{60}. According to classical models that compute the charge state of large molecules in space, C_{60} is expected to be mostly neutral in the diffuse ISM. This is in agreement with the abundances of diffuse C_{60} we derive here from observations.

Key words. infrared: ISM – ISM: molecules – ISM: lines and bands

1. Introduction

Fullerenes are cage-like macromolecules made of carbon. The most emblematic member of this family, C_{60}, i.e. buckminsterfullerene, was serendipitously discovered by Kroto et al. (1985) during experiments aimed at simulating carbon chemistry in the atmospheres of evolved stars. Fullerenes have been extensively studied in the field of chemistry because of their unique properties and potential applications for nanotechnologies. Soon after the discovery of these macromolecules, it was recognized that fullerenes could be present in space and constitute a family of species relevant to astrochemistry (Kroto et al. 1985; Kroto & Jura 1992). In particular, it was postulated that their electronic transitions could be at the origin of some of the numerous unidentified absorption bands observed towards reddened stars, the so-called diffuse interstellar bands (DIBs). Foing & Ehrenfreund (1994) proposed that two DIBs at 9577 and 9632 Å could be due to the C_{60} cation, C_{60}^+, but this proposal could not be confirmed at that time because of the lack of gas-phase laboratory spectroscopy. Clear evidence for the presence of fullerenes (C_{60}, C_{60}^+, C_{70}) in space was provided recently with the detection of infrared (IR) emission bands of fullerenes in regions with intense UV radiation such as evolved stars (e.g. Cami et al. 2010; García-Hernández et al. 2010) and star-forming regions (Sellgren et al. 2010; Roberts et al. 2012; Berné et al. 2013; Castellanos et al. 2014). In parallel, new gas-phase laboratory experiments (Campbell et al. 2015) provided an accurate wavelength determination of the electronic transitions of C_{60}^+, which were found to be in excellent agreement with observations, therefore supporting the hypothesis that the 9577 and 9632 Å DIBs are due to the presence of C_{60}^+ in the diffuse interstellar medium (ISM). If fullerenes are present in the diffuse ISM, they should absorb ultraviolet (UV) photons

and re-emit their energy in the IR, hence their IR vibrational bands should be observed. Unfortunately, in the diffuse ISM, the exciting UV radiation field is orders of magnitude smaller compared to star-forming regions, resulting in extremely weak IR fluorescence. For this reason fullerene emission has not been detected there so far, precluding an independent confirmation of their presence in this environment.

2. Observations

We retrieved archival IR spectra obtained with the InfraRed Spectrograph (IRS; Houck et al. 2004) on board *Spitzer* (Werner et al. 2004a) towards two lines of sight. To complement this data, we used the ISOCAM (Cesarsky et al. 1996) data, which was published in Flagey et al. (2006). An overview of the studied regions and data are presented in Fig. 1.

The first line of sight (Fig. 1, left column, Chamaeleon), corresponds to a translucent cloud that is situated on the frontside of the Chamaeleon complex at a distance of ∼70 pc (Mizuno et al. 2001). As can be seen from the HI and CO spectra (Fig. 1), this is a single cloud. The physical conditions for this cloud have been derived by Ingalls et al. (2011) based on the study of the molecular hydrogen emission: the hydrogen density is ∼30−100 particles cm^{-3} and the ultraviolet (UV) radiation field there is in the range of $G_0 = 0.7-3$ (with $G_0 = 1$ corresponding to 1.2×10^{-7} W m^{-2} sr^{-1}, the interstellar standard radiation field calculated by Habing 1968). The data for this line of sight consists of low resolution spectroscopy ($\lambda/\Delta \lambda \sim 60-100$) covering the 5−35 μm range and published in Ingalls et al. (2011) who focused on H$_2$ emission. The second line of sight (Fig. 1, right column, Scutum) corresponds to a diffuse Galactic region, free of star formation, situated close to the Scutum. As can be seen in the HI and CO spectra presented in Fig. 1, this line of
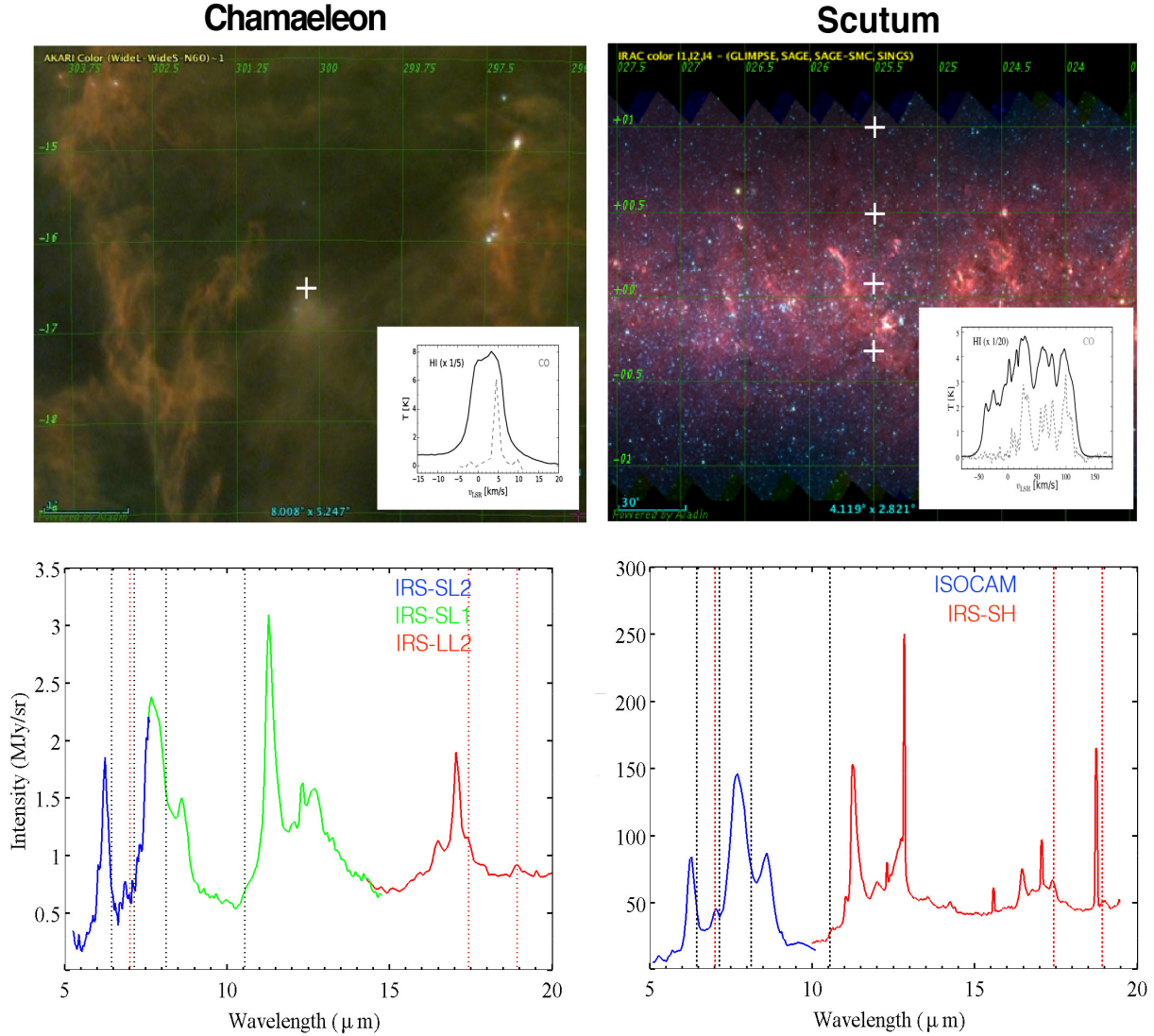
Chamaeleon

Scutum

Fig. 1. *Upper panels*: images of the Chamaeleon (translucent) and Scutum (diffuse) lines of sight studied in this article, observed with *Spitzer*-IRAC (Werner et al. 2004a; Fazio et al. 2004). Positions of the spectroscopic observations are indicated with white crosses. The images show IRAC colours red = 8.0 μm, green = 4.5 μm, and blue = 3.6 μm. *Inserts* show the HI and CO emission spectra (McClure-Griffiths et al. 2009; Dame et al. 2001; Boulanger et al. 1998). *Lower panels*: mid-infrared spectra towards the studied lines of sight are represented. The vertical lines indicate the positions of C_{60} (red) and C_{60}^{+} (black) bands observed in the NGC 7023 reflection nebula (Sellgren et al. 2010; Berné et al. 2013). The band at 7.0 μm observed in the diffuse line of sight is due to [ArII].

Table 1. Properties of the studied lines of sight.

	Chamaeleon	Scutum	Refs.
Coord. (Gal. / deg.)	+300.13, −16.49	26.47, −0.3– +1.0	(1), (2)
UV field G_0*	0.7−3	1−10	(1), (3)
N_H (H cm^{-2})	2.7−5.6 × 10^{21}	5.7 × 10^{22}	(1), (3)
A_V** (mag)	1.4−3.0	30.5	−
Comment	Single translucent cloud	Multiple clouds	−

Notes. $^{(*)}G_0 = 1$ corresponds to a UV field of 1.2×10^{-7} W m^{-2} sr^{-1}. $^{(**)}$ Computed using $N_H/A_V = 1.87 \times 10^{21}$ for Scutum (value for the diffuse ISM) and $N_H/A_V = 3.1 \times 10^{21}$ for the Chamaelon (value for translucent/dense ISM).

References. (1): Ingalls et al. (2011); (2): this work; (3): Falgarone et al. (2005).

sight probes several clouds, where hydrogen can be in molecular, atomic, or ionized form. Falgarone et al. (2005) studied this region of the Galaxy in detail using ISO spectroscopy and were able to decompose the line of sight into several density components. The radiation field on this line of sight varies between

$G_0 = 1$ and $G_0 = 10$ (Falgarone et al. 2005). The *Spitzer* spectroscopic data for this line of sight was not previously published; it consists of medium resolution spectroscopy ($\lambda/\Delta \lambda \sim 600$) covering the 9−20 μm range. For both lines of sight, we reduced the data starting from the basic calibrated data and carefully
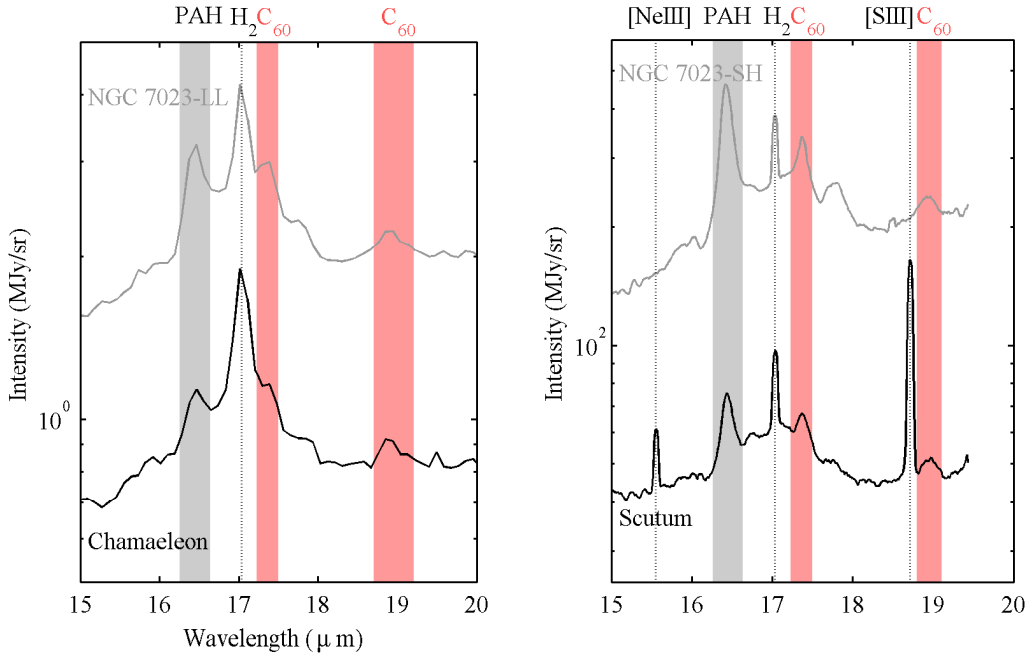
Fig. 2. Mid-infrared spectra extracted over the $15-20\,\mu m$ range for both lines of sight (see Appendix A for details). The spectrum of the NGC 7023 nebula where C_{60} emission has been reported (Sellgren et al. 2010) is shown as a reference. The Chamaeleon spectrum is compared with a low resolution spectrum (IRS-LL) of NGC 7023, while the Scutum line of sight spectrum is compared to a medium resolution spectrum (IRS-SH) of NGC 7023, to be consistent with the observing modes used to obtain the spectra of interest here (see Appendix A). The positions of the C_{60} vibrational bands are indicated with red vertical patches. The 16.4 μm attributed to PAH emission is indicated with a grey patch. Spectrally unresolved lines of molecular hydrogen and ions are also indicated with vertical dotted lines.

subtracting background emission (see Appendix A). The extracted mid-IR spectra over the full spectral range for the two lines of sight are presented in Fig. 1.

In Fig. 2, the same spectra are shown over a smaller spectral range that is of interest when searching for the emission of C_{60}. For comparison, the spectra of the NGC 7023 massive star-forming region are shown, where C_{60} was detected by Sellgren et al. (2010) and where the UV radiation field is much higher, i.e. $G_0 = 1000-10\,000$. The diffuse and translucent cloud spectra show a number of broad features, which are commonly attributed to the emission of large carbonaceous molecules i.e. polycyclic aromatic hydrocarbons (PAH; Tielens 2008). The ratio between the 11.2 and 7.7 μm PAH bands observed in both lines of sight is compatible with PAHs being mostly neutral (Pilleri et al. 2012). The molecular hydrogen lines at 17.0 μm and 12.3 μm are also observed towards both lines of sight. In addition, ionic lines from the warm ionized medium are detected towards the Scutum line of sight. The two most intense bands of C_{60}, situated at 17.4 and 18.9 μm, are clearly detected in both lines of sight (Fig. 2)[1]. The vibrational spectrum of C_{60} is characterized by two additional weaker bands at 7.0 and 8.5 μm, which are not detected. However this non-detection is consistent with the noise level that exceeds the expected intensity for these bands. The 18.9 μm band is detected at a level that is 3.2 and 12.2 times above the root mean square noise, for the Chameleon cloud and for the Scutum line of sight, respectively. The strongest bands of C_{60}^+ (at 6.4 and 7.1 μm, Berné et al. 2013) are not detected. C_{60}^+ also has an emission band close to 18.9 μm, which could correspond to the emission band detected the spectra in Fig. 2, but we show in Appendix F that C_{60}^+ cannot contribute more than ~25% to the observed band.

---

[1] The 17.4 μm can be contaminated by emission from polycyclic aromatic hydrocarbons.

3. Abundances of C_{60}

Using the integrated intensity of the 18.9 μm band of C_{60} and information reported in Table 1, it is possible to estimate an abundance for C_{60} in both lines of sight (see Appendix B). The values found are of the order of a few 10^{-4} to a few 10^{-3} of the gas-phase carbon locked in C_{60} (Table 2). This can be compared to the abundances of C_{60}^+ for the diffuse ISM derived from DIB measurements. Using the recent laboratory measurements for the oscillator strength of C_{60}^+ electronic transitions (Campbell et al. 2016), we derived the abundance of C_{60}^+ towards lines of sight where the 9577 Å DIB has been detected (Appendix C). These abundances are in the range of $0.6-1.1 \times 10^{-3}$ of the carbon (Table C.1), i.e. comparable to what is found for C_{60} in this study; they are also in agreement with the upper limit for the abundance of C_{60}^+ we derived from the non-detection of the infrared bands of this species of 1.8×10^{-3} of the carbon (see Appendix D). Abundances for C_{60} in the diffuse ISM, star-forming regions and evolved stars are summarized in Table 2. Fullerenes are most abundant in carbon-rich evolved stars, roughly an order of magnitude less abundant in the diffuse ISM, and two orders of magnitude less abundant in star forming regions. It should however be noted that C_{60} is detected towards only ~3% of the evolved stars observed with *Spitzer* (Otsuka et al. 2014). Overall, the relatively large abundance of C_{60} in the diffuse ISM may therefore reflect the long-term processing of carbonaceous material by UV photons of massive stars, which can lead to the formation of fullerenes (Berné & Tielens 2012; Berné et al. 2015).

According to classical theoretical models for the charge state of large molecules in space, C_{60} should be mostly neutral for standard physical conditions of the diffuse ISM. Bakes & Tielens (1995) computed the charge distribution for the specific case of C_{60} in the diffuse ISM and find that ~30% is

Table 2. Abundances of fullerenes (% of gas-phase carbon locked in species), derived from emission or absorption measurements in star-forming regions and in the diffuse ISM and evolved stars.

	Emission	Absorption
	Star-forming regions	
C_{60}^+	0.01^*	−
C_{60}	$0.04-0.06^{**}$	−
	Diffuse ISM	
C_{60}^+	0.2 *,†	$0.06-0.1^\star$
C_{60}	$0.03-0.4^\star$	−
	Evolved stars	
C_{60}^+	−	1.2 **
C_{60}	$0.1-3.0^{\star\star\star}$	−

Notes. $^{(*)}$ From Berné et al. (2013); $^{(**)}$ from Castellanos et al. (2014); $^{(\star)}$ This work, see Appendices B–D; $^{(\dagger)}$ upper limit; $^{(\star\star)}$ From Iglesias-Groth & Esposito (2013), for one source only; $^{(\star\star\star)}$ from Cami et al. (2011) and references therein.

anionic, ∼60% is neutral, and ∼10% is cationic. These numbers are compatible with the absolute abundances summarized in Table 2, which point to a (not very restrictive) C_{60} over C_{60}^+ ratio ranging between 0.3 to 6. C_{60}^- is expected to be abundant in models and hence could be searched for in space. The strongest vibrational bands of C_{60}^- are around 17.5 and 7.3 μm (Kupser et al. 2008). The 17.5 μm band is difficult to identify because of the presence of PAH emission at 17.4 μm. A band at 7.3 μm seems present in the spectrum of the Chamaeleon line of sight, however this region of the spectrum is quite noisy and higher sensitivity data will be required to confirm this. Observations of diffuse lines of sight with the *James Webb* Space Telescope, which has the sensitivity to detect C_{60} and C_{60}^+ as well as tracers of the diffuse ISM should allow us to conduct more detailed studies on the charge balance of C_{60} in the diffuse ISM. Laboratory studies to quantify key molecular parameters involved, such as the electron recombination rate of C_{60}^+, are also required.

Finally, the detection of C_{60} IR emission bands in the diffuse ISM suggests that the electronic transitions of this molecules could be identified in absorption. However, given their low oscillator strengths, this will be challenging as we illustrate in Appendix E.

4. Conclusion

In the past few years, our understanding of the organic inventory in space has greatly benefited from studies of the infrared emission of the Galaxy, in particular with the first identifications of fullerenes. Meanwhile, the field of diffuse interstellar bands has been reinvigorated by the convincing assignment of the 9577 and 9632 Å DIBs to the electronic transitions of C_{60}^+. The detection of C_{60}^+ IR emission in the diffuse ISM, with the same abundance as those derived from studies in absorption, would provide a strong independent confirmation of the DIB assignment. It is also likely that astronomical observations combining vibrational and electronic spectroscopy through the detection of emission and absorption bands, with the support of laboratory and theoretical investigations, can help identify new species and cast a new light on the DIB conundrum and the organic inventory in space. The detailed spectroscopy of C_{60} and C_{60}^+, which are isolated in the diffuse ISM, can also offer the possibility to study some of the fundamental molecular properties of these species in synergy with laboratory and theoretical investigations.

References

Bakes, E., & Tielens, A. 1995, in The Diffuse Interstellar Bands, eds. A. G. G. M. Tielens, & T. P. Snow, Astrophys. Space Sci. Lib., 202, 315
Berné, O., & Tielens, A. G. G. M. 2012, Proc. Nat. Acad. Sci., 109, 401
Berné, O., Mulas, G., & Joblin, C. 2013, A&A, 550, L4
Berné, O., Montillaud, J., & Joblin, C. 2015, A&A, 577, A133
Boulanger, F., Bronfman, L., Dame, T. M., & Thaddeus, P. 1998, A&A, 332, 273
Cami, J., Bernard-Salas, J., Peeters, E., & Malek, S. E. 2010, Science, 329, 1180
Cami, J., Bernard-Salas, J., Peeters, E., & Malek, S. E. 2011, in The Molecular Universe, eds. J. Cernicharo, & R. Bachiller, IAU Symp., 280, 216
Campbell, E. K., Holz, M., Gerlich, D., & Maier, J. P. 2015, Nature, 523, 322
Campbell, E. K., Holz, M., Maier, J. P., et al. 2016, ApJ, 822, 17
Castellanos, P., Berné, O., Sheffer, Y., Wolfire, M. G., & Tielens, A. G. G. M. 2014, ApJ, 794, 83
Cesarsky, C. J., Abergel, A., Agnese, P., et al. 1996, A&A, 315, L32
Cox, N. L. J., Cami, J., Kaper, L., et al. 2014, A&A, 569, A117
Dame, T. M., Hartmann, D., & Thaddeus, P. 2001, ApJ, 547, 792
Diplas, A., & Savage, B. D. 1994, ApJS, 93, 211
Falgarone, E., Verstraete, L., Pineau Des Forêts, G., & Hily-Blant, P. 2005, A&A, 433, 997
Fazio, G. G., Hora, J. L., Allen, L. E., et al. 2004, ApJS, 154, 10
Flagey, N., Boulanger, F., Verstraete, L., et al. 2006, A&A, 453, 969
Foing, B. H., & Ehrenfreund, P. 1994, Nature, 369, 296
García-Hernández, D. A., Manchado, A., García-Lario, P., et al. 2010, ApJ, 724, L39
Habing, H. J. 1968, Bull. Astron. Institutes of The Netherlands, 19, 421
Herbig, G. H. 2000, ApJ, 542, 334
Houck, J. R., Roellig, T. L., van Cleve, J., et al. 2004, ApJS, 154, 18
Iglesias-Groth, S., & Esposito, M. 2013, ApJ, 776, L2
Ingalls, J. G., Bania, T. M., Boulanger, F., et al. 2011, ApJ, 743, 174
Kroto, H. W., & Jura, M. 1992, A&A, 263, 275
Kroto, H. W., Heath, J. R., Obrien, S. C., Curl, R. F., & Smalley, R. E. 1985, Nature, 318, 162
Kupser, P., Steill, J. D., Oomens, J., Meijer, G., & von Helden, G. 2008, Phys. Chem. Chem. Phys., 10, 6862
McClure-Griffiths, N. M., Pisano, D. J., Calabretta, M. R., et al. 2009, ApJS, 181, 398
Menéndez, J., & Page, J. B. 2000, Vibrational spectroscopy of C60, eds. M. Cardona & G. Güntherodt (Berlin, Heidelberg: Springer), 27
Mizuno, A., Yamaguchi, R., Tachihara, K., et al. 2001, Proc. Astron. Soc. Japan, 53, 1071
Omont, A. 2016, A&A, 590, A52
Otsuka, M., Kemper, F., Cami, J., Peeters, E., & Bernard-Salas, J. 2014, MNRAS, 437, 2577
Pilleri, P., Montillaud, J., Berné, O., & Joblin, C. 2012, A&A, 542, A69
Roberts, K. R. G., Smith, K. T., & Sarre, P. J. 2012, MNRAS, 421, 3277
Sassara, A., Zerza, G., Chergui, M., & Leach, S. 2001, ApJ, 135, 263
Sellgren, K., Werner, M. W., Ingalls, J. G., et al. 2010, ApJ, 722, L54
Smith, J. D. T., Armus, L., Dale, D. A., et al. 2007, PASP, 119, 1133
Sofia, U. J., Lauroesch, J. T., Meyer, D. M., & Cartledge, S. I. B. 2004, ApJ, 605, 272
Strelnikov, D., Kern, B., & Kappes, M. M. 2015, A&A, 584, A55
Tielens, A. G. G. M. 2008, ARA&A, 46, 289
Walker, G. A. H., Bohlender, D. A., Maier, J. P., & Campbell, E. K. 2015, ApJ, 812, L8
Werner, M. W., Roellig, T. L., Low, F. J., et al. 2004a, ApJS, 154, 1
Werner, M. W., Uchida, K. I., Sellgren, K., et al. 2004b, ApJS, 154, 309
Wilson, O. C., & Merrill, P. W. 1937, Contributions from the Mount Wilson Observatory/Carnegie Institution of Washington, 570, 1

Appendix A: Data analysis

The data was retrieved from the *Spitzer* science archive[2]. We used the data at the basic calibrated level (bcd) for both lines of sight. The astronomical observation request (AOR) keys for these observations are, for the four positions of the Scutum line of sight (LoS): 11060992, 12544768, 11061504, 11061760, from the programme 3513 (PI E. Falgarone), and for the Chamaeleon LoS 28315392, from programme 491 (PI J. Ingalls). The off positions were included in this latter programme, and for the former observations, we used the offs performed the same day for extragalactic sources by another programme (programme 1420; PI L. Armus). The off subtraction, in both cases, was performed at the .bcd level, i.e. before building the 3D spectral cubes. The data reduction was achieved using the CUBISM software (Smith et al. 2007), including the slit loss correction function algorithm[3]. Once the cubes were built, the spectra were obtained by averaging the spectral cubes over all the spatial positions to improve the signal to noise ratio.

The complementary data from NGC 7023 has been discussed extensively in the literature, it was first presented by Werner et al. (2004b). The positions we use to extract the reference spectra are rectangles whose vertices coordinates are given hereafter: for the low resolution spectrum (LL) used in the comparison with the translucent cloud spectrum (21:01:40.579, +68:10:42.96; 21:01:42.343, +68:10:54.6; 21:01:40.255, +68:11:04.44; 21:01:38.491,+68:10:52.80), and for the medium resolution spectrum (SH) used in the comparison with the diffuse ISM spectrum (21:01:24.800, +68:10:11.50; 21:01:32.368, +68:09:33.95; 21:01:40.448, +68:10:24.60; 21:01:32.880,+68:11:02.16). The LL spectrum was extracted in the north-west photodissociation region (PDR) of the nebula, where rotational H_2 emission is observed to be strong, i.e. at the surface of the molecular cloud. The high resolution spectrum was obtained by averaging the spectral cube over a region that covers the north-west PDR and the cavity of atomic gas situated close to the illuminating star HD 200775.

Appendix B: Derivation of neutral C_{60} abundances from the infrared emission

The derivation of the C_{60} abundance performed here relies on the assumption that the energy absorbed by C_{60} in the UV is completely re-radiated in the IR bands. For moderate internal energies ($\sim 5-15$ eV), such as those of C_{60} molecules excited by Far-UV photons in the ISM, the main relaxation channel is indeed IR emission (see Fig. 2 in Berné et al. 2015) and this assumption is valid. The total IR intensity in W m^{-2} sr^{-1} emitted by C_{60} molecules is hence,

$$I_{tot} = N(C_{60}) \times \sigma_{UV} \times G_0 \times 1.2 \times 10^{-7}, \quad (B.1)$$

where $N(C_{60})$ is the column density of C_{60}, σ_{UV} is the UV absorption cross section of C_{60} which we take to be 4.2×10^{-16} cm^2 following Berné & Tielens (2012), and G_0 is the radiation field (see Table 1). Unfortunately, in our observations, the bands at shorter wavelengths (7.0 and 8.5 μm) are not detected, and the 17.4 μm band is contaminated by PAH emission, hence I_{tot} cannot be derived directly. Instead, it can be estimated using the 18.9 μm band intensity ($I_{18.9}$), assuming that $I_{tot} = 2.3 \times I_{18.9}$, which is what is observed in NGC 7023 (Berné et al. 2013). This

assumption is valid considering that the band ratios of the IR bands of C_{60} depend on the average energy of absorbed UV photons that are expected to be comparable in NGC 7023 and in the diffuse ISM, since both environments are dominated by the UV fields of young massive stars. Hence, one can solve Eq. (B.1) for $N(C_{60})$, and derive the abundance of C_{60} relative to carbon as follows:

$$f_C^{C_{60}} = \frac{N(C_{60}) \times 60}{N(H) \times [C]}, \quad (B.2)$$

adopting a carbon-to-hydrogen fraction measured in the diffuse ISM, i.e. [C] $= 1.6 \times 10^{-4}$ (Sofia et al. 2004), and the values for $N(H)$ in Table 1. For the specific cases considered here, we derive $I_{18.9} = 2.5 \times 10^{-10}$ and $I_{18.9} = 1.2 \times 10^{-8}$ W m^{-2} sr^{-1} for the Chamaeleon and Scutum LoS respectively. Using Eqs. (B.1), (B.2) and the values in Table 1 (including uncertainties on the hydrogen column density and radiation field) yields abundances of C_{60} of $0.3-2.4 \times 10^{-3}$ and $0.4-3.6 \times 10^{-3}$ of the gas-phase carbon locked in C_{60}, for the Chamaeleon and Scutum LoS, respectively.

Appendix C: C_{60}^+ abundances in the diffuse interstellar medium

The fraction of carbon locked in C_{60}^+ relative to gas-phase carbon is given by

$$f_C^{C_{60}^+} = \frac{N(C_{60}^+) \times 60}{N(H) \times [C]}, \quad (C.1)$$

adopting a carbon-to-hydrogen fraction measured in the diffuse ISM, [C] $= 1.6 \times 10^{-4}$. Values of the column density of C_{60}^+, $N(C_{60}^+)$, were derived in previous works along several diffuse ISM LoS along which the two DIBs at 9577 and 9632 Å were observed. In Table C.1, we report the values for three well-studied LoS and derived abundances for C_{60}^+ using the equation above. The derived values are of the order of a few 10^{-3} of the gas-phase carbon. Omont (2016) finds an average value of the fraction of carbon contained in C_{60}^+ (with respect to the total carbon abundance, including dust) $X(C_{60}^+) = 4 \pm 2 \times 10^{-4}$, equivalent to $f_C^{C_{60}^+} \sim 1 \times 10^{-3}$ of the gas phase carbon, in agreement with our results.

Appendix D: C_{60}^+ infrared emission upper limit

It is possible to derive a limit for the abundance of C_{60}^+ based on the infrared spectra of the Chamaeleon and Scutum LoS using the same approach as for C_{60} (see appendix B). The 7.1 μm band of C_{60}^+ is the easiest to detect (Berné et al. 2013), however it is absent in both lines of sight (Fig. 1). Based on these non-detections, we can place an upper limit on $I_{7.1}$, which we can convert into an I_{tot} for C_{60}^+ using the band ratio observed in NGC 7023 (Berné et al. 2013). We derive an upper limit for the C_{60}^+ column density, which we convert into an abundance using Eq. (B.2). Using the equation of energy budget (Eq. (B.1)) and assuming a similar value of the UV absorption cross section for C_{60} and C_{60}^+, we can derive an upper limit for the C_{60}^+ column density, which we convert into an abundance using Eq. (C.1). This yields an upper limit for the C_{60}^+ abundance of 3×10^{-3} of the elemental carbon abundance in the Chamaeleon line of sight and $\sim 1.8 \times 10^{-3}$ of the carbon for the Scutum line of sight. Both limits are above the measurements of C_{60}^+ abundance resulting from the detection of the electronic transitions (Table C.1).

Table C.1. C_{60}^+ column densities and abundances (fraction of gas-phase carbon) for several well-studied diffuse ISM lines of sight.

Line of sight	$N(C_{60}^+)^*$	Ref. for 9577 DIB EW	$N(H)^{**}$	C_{60}^+ abundance f_C
HD169454	0.9×10^{13}	Walker et al. (2015)	3×10^{21}	1.1×10^{-3}
HD183143	2×10^{13}	Walker et al. (2015)	7.4×10^{21}	1.0×10^{-3}
4U1907+09	2.6×10^{13}	Cox et al. (2014)	1.7×10^{22}	6.0×10^{-3}

Notes. [*] Column density computed from the measured equivalent width via the measured cross sections given by Campbell et al. (2016). [**] Hydrogen column density, $N(H) = N(HI + 2 N(H_2))$, from direct measurements (HD 169454: Diplas & Savage 1994) or visual extinction, A_V (other sightlines; see text for details).

Table E.1. Wavelength, oscillator strength, and FWHM of the considered C_{60} electronic bands (all values from Sassara et al. 2001).

λ (Å)	f	$FWHM$ (Å)
3980	0.007	5.5
4024	0.005	4.0

Appendix E: Prediction of neutral C_{60} DIB strength

The detection of the IR emission of neutral C_{60} in the diffuse ISM with abundances comparable to C_{60}^+ suggests that this molecule could be a DIB carrier. Using the abundances derived in this paper and relevant data for the positions, strength, and widths of the electronic transitions of C_{60} (Sassara et al. 2001, Table E1), it is possible to compute the predicted depth of the electronic transitions of neutral C_{60}. Truly accurate positions, oscillator strengths, and band widths have not yet been determined for the electronic absorption bands of neutral C_{60} in the gas phase at low temperatures, which could therefore be shifted by several Å with respect to these recommended values. We use the following relation between column density, N, and equivalent width, EW in Å (Wilson & Merrill 1937):

$$EW = \frac{N f \lambda^2}{1.13 \times 10^{20}}, \tag{E.1}$$

where λ is the band position (in Å) and f its oscillator strength (cf. Table E.1).

For a Gaussian profile the central depth, τ_0, of the line centre relative to the local continuum, is given as

$$\tau_0 = \frac{EW}{1.571 \times FWHM}. \tag{E.2}$$

For the diffuse Scutum LoS, the column density derived from infrared emission is $N(C_{60}) = 5.6 \times 10^{14}$ cm^{-2} for a sightline with total visual extinction, A_V, of 30.5 magnitudes. For the Chamaeleon LoS, with $A_V = 1$–2 mag, we have $N(C_{60}) = 1.7 \times 10^{13}$ cm^{-2}. We can thus infer $N(C_{60}) \sim 1 \times 10^{13}$ cm$^{-2}/A_V$ from both sightlines. Using Eqs. (E.1) and (E.2), this yields central depths of ~0.1% per unit visual extinction. These low values are inherent to the rather low oscillator strengths of the C_{60} electronic transitions and suggest that C_{60} is unlikely to be responsible for strong DIBs, which can be several percent of the continuum (Herbig 2000). However, weak DIBs, which can be detected thanks to highly sensitive spectroscopy, could well be attributed to C_{60} with the help of new gas-phase laboratory spectroscopy to provide accurate positions, width, and strengths

for the electronic transitions. For instance, on the Scutum LoS, the predicted equivalent width for the C_{60} DIBs with the number quoted above is of the order of 200 mÅ provided one can find a proper background star.

Appendix F: Possible contribution of C_{60}^+ to the 18.9 μm band

C_{60}^+ is known to have an infrared vibrational band at a wavelength close to the strongest band of C_{60}, i.e. at ~18.9 μm (see theoretical calculations in Berné et al. 2013, and experimental data in Strelnikov et al. 2015). Based on the upper limits for the 7.1 μm band (Fig. 1), it is possible to derive an estimate of the maximum contribution of C_{60}^+ to the 18.9 μm band (Fig. 2). A proper analysis would require a detailed emission model, including a description of the UV field, absorption, excitation, and cooling of the molecules. Here we consider a simplified model. From the observed ratio between the 7.0 and 18.9 μm bands of C_{60} in NGC 7023 (Sellgren et al. 2010), we can derive a mean colour temperature T_C such that

$$\frac{I_{7.0}}{I_{18.9}} = 0.83 = \frac{\sigma_{C_{60}}(7.0) \times B(7.0, T_C)}{\sigma_{C_{60}}(18.9) \times B(18.9, T_C)}, \tag{F.1}$$

where $B(\lambda)$ is the Planck function and σ is the infrared cross section of the molecule. Applying a similar reasoning for C_{60}^+ and assuming the same colour temperature for both C_{60} and C_{60}^+, the ratio between the 7.1 and 18.9 μm features reads

$$\frac{I_{7.1}}{I_{18.9}} = \frac{\sigma_{C_{60}^+}(7.1) \times B(7.1, T_C)}{\sigma_{C_{60}^+} 18.9 \times B(18.9, T_C)} = \frac{\sigma_{C_{60}^+}(7.1) \times \sigma_{C_{60}}(18.9)}{\sigma_{C_{60}^+}(18.9) \times \sigma_{C_{60}}(7.0)} \times 0.83. \tag{F.2}$$

Using the IR cross sections for C_{60} and C_{60}^+ of Menéndez & Page (2000) and Strelnikov et al. (2015), respectively, yields a theoretical value of $I_{7.1}/I_{18.9} \sim 9$. The upper limits for the 7.1 μm band in the Chamaeleon and Scutum LoS are 5.9×10^{-10} and 1.2×10^{-8} W m^{-2} sr^{-1}, respectively. This results in a maximum contribution of C_{60}^+ to the 18.9 μm band of 6.6×10^{-11} and 1.3×10^{-9} W m^{-2} sr^{-1}, respectively. This is to be compared to the observed emissions of the 18.9 μm band of 2.5×10^{-10} and 1.2×10^{-8} W m^{-2} sr^{-1}. Hence, the contribution of C_{60}^+ to the 18.9 μm band is at most ~25 and 10% in the Chamaeleon and Scutum LoS, respectively. In any case, the major contributor to the 18.9 μm band is C_{60}.